Paradoxical noise preference in RNNs

Anonymous authors
Paper under double-blind review

Abstract

In recurrent neural networks (RNNs) used to model biological neural networks, noise is typically introduced during training to emulate biological variability and regularize learning. The expectation is that removing the noise at test time should preserve or improve performance. Contrary to this intuition, we find that continuous-time recurrent neural networks (CTRNNs) often perform best at a nonzero noise level—specifically, the same level used during training. This noise preference typically arises when noise is injected inside the neural activation function; networks trained with noise injected outside the activation function perform best with zero noise. Through analyses of simple function-approximation, maze-navigation, and single-neuron regulator tasks, we show that the phenomenon stems from noise-induced shifts of fixed points (stationary distributions) in the underlying stochastic dynamics of the RNNs. These fixed point shifts are noise-level dependent and bias the network outputs when the noise is removed, degrading performance. Analytical and numerical results show that the bias arises when neural states operate near activation-function nonlinearities, where noise is asymmetrically attenuated, and that performance optimization incentivizes operation near these nonlinearities. Thus, networks can overfit to the stochastic training environment itself rather than just to the input–output data. The phenomenon is distinct from stochastic resonance, wherein nonzero noise enhances signal processing. Our findings reveal that training noise can become an integral part of the computation learned by recurrent networks, with implications for understanding neural population dynamics and for the design of robust artificial RNNs.

1 Introduction

Recurrent neural networks (RNNs) are central in computational neuroscience as models of population-level computation (Güçlü & Van Gerven, 2017; Yang & Molano-Mazón, 2021; Barak, 2017; Driscoll et al., 2024; Yang et al., 2019; Wang et al., 2021). Noise is commonly introduced at training of these RNNs (e.g., Yang et al. (2019); Driscoll et al. (2024)) to mimic biological synaptic noise (Faisal et al., 2008) and regularize learning (Lim et al., 2021). Such noise promotes stable training and reduces sensitivity to individual neural activities or weights, discouraging sharp minima and effectively acting as a complexity penalty (Bishop, 1995; You et al., 2019; Noh et al., 2017; Lim et al., 2021). If noise served only as regularization, removing it at test time should maintain or improve performance. Contrary to this expectation, we find that continuous-time recurrent neural networks (CTRNNs; Yang et al. (2019); Driscoll et al. (2024), figure 1) perform best at a nonzero noise level, typically matching the training noise. Thus, the networks develop a preference for a particular noise level. We analyze the dynamical basis of this noise preference, showing it arises from how noise shifts the stationary distributions of the underlying stochastic dynamics. We examine different noise injection schemes to identify conditions under which a preference naturally develops. Though reminiscent of stochastic resonance-like phenomena in which noise enhances signal processing (Katada & Nishimura, 2009; Metzner et al., 2024; Krauss et al., 2019), our noise preference phenomenon is mechanistically distinct, implying that noise-facilitated behavior may have a broader computational role in neural systems.

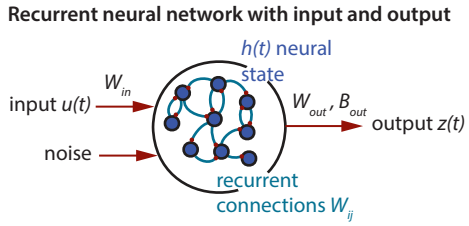

Figure 1: A continuous-time recurrent neural network with input and output at each time. Variants of this network are used in computational neuroscience Yang et al. (2019); Driscoll et al. (2024), and the effect of synaptic noise on such networks is studied here.

2 Methods

2.1 CTRNN architecture

CTRNNs (figure 1) implement ordinary differential equations that coarsely model synaptic interactions among a population of biological neurons (Barak, 2017; Yang et al., 2019; Driscoll et al., 2024). Their internal dynamics are usually described by the equation:

$$\tau \frac{dh}{dt} = -h + f(W_{\text{rec}}h + W_{\text{in}}u + B_{\text{in}} + \sigma_{\text{in}}\eta), \tag{1}$$

where $h \in \mathbb{R}^n$ is a vector denoting the neural state (i.e., the state of the network), usually modeling neuronal firing rates in biological networks (Yang et al., 2019), n is the number of neurons, $\tau \in \mathbb{R}$ is the neural time constant, $W_{\text{rec}} \in \mathbb{R}^{n\times n}$ is the recurrent weight matrix, $u \in \mathbb{R}^m$ is the vector containing various inputs (e.g., sensory feedback, task identity), $W_{\text{in}} \in \mathbb{R}^{n\times m}$ is the input weight matrix, $B_{\text{in}} \in \mathbb{R}^n$ is the neural bias vector, $\sigma_{\text{in}}\eta \in \mathbb{R}^n$ is a Gaussian white noise process with variance σ_{in}^2 along all dimensions, and $f(\cdot)$ is a scalar nonlinear activation function, applied element-wise over vector arguments. The networks produce outputs $z \in \mathbb{R}^p$ via an affine transform $z = W_{\text{out}}h + B_{\text{out}}$, where $W_{\text{out}} \in \mathbb{R}^{p\times n}$ and $B_{\text{out}} \in \mathbb{R}^p$ are the output weight matrix and bias vector, respectively.

To simulate these networks, we integrate Equation 1 by Euler's method (as in Yang et al. (2019) and others), giving the discrete time equation:

$$h_{t+1} = (1-\gamma)h_t + \gamma f(W_{\text{rec}}h_t + W_{\text{in}}u_t + B_{\text{in}} + \mathcal{N}(0, \sigma_{\text{in}}^2)), \tag{2}$$

where $\gamma = \Delta t/\tau$ is a non-dimensional ratio of Δt, the discrete timestep, and τ, the neural time constant, and σ_{in} is the standard deviation of the injected noise, which is sampled independently for each neuron in each timestep. Unless otherwise stated, we used $\tau = 0.1$ and $\Delta t = 0.02$, resulting in $\gamma = 0.2$. For $f(\cdot)$, we use rectifying activation functions, either ReLU, or its smooth approximation, SoftPlus.

As presented thus far, the noise is injected inside the activation function, as is common in the computational neuroscience literature (e.g., Yang et al. (2019); Driscoll et al. (2024)). This placement ensures positivity of the neural state h, facilitating their interpretation as firing rates. For didactic purposes, we also consider a variant of Equation 2 with the noise added outside the activation function:

$$h_{t+1} = (1-\gamma)h_t + \gamma(f(W_{\text{rec}}h_t + W_{\text{in}}u_t + B_{\text{in}}) + \mathcal{N}(0, \sigma_{\text{out}}^2)). \tag{3}$$

We refer to networks trained with noise injected inside and outside their activation functions as noise-in and noise-out networks, respectively, and we refer to their noise as either pre-activation noise (for noise-in networks) or post-activation noise (for noise-out networks).

2.2 Tasks for illustrating the effect of noise

To study the effect of noise in CTRNNs (Figure 1), we trained both noise-in and noise-out variants on simple tasks and evaluated their performance, focusing on whether or not there is a nonzero noise level for

optimal performance at test time. We mainly focus on a simple function approximation task to illustrate the phenomenon, but we also include a single-neuron regulator task to build intuition and a more complex maze navigation task to test whether the results we see in these simpler tasks are general enough to apply in a more neuroscientifically relevant context. All three are supervised learning tasks, trained by minimizing a mean squared error loss function; see Appendix A for further training details. We provide the essential elements of the three tasks in the remainder of this section; see Appendix B for detailed equations and implementation information.

2.2.1 Function computation tasks

In the function computation tasks, we require the neural networks to compute univariate functions ($g(x)$, $x \in \mathbb{R}$, $g(x) \in \mathbb{R}$) over some compact interval. The networks receive a constant one-dimensional input x for the argument of the function being approximated, and the network output at the end of a "computation" period must match the corresponding value of the function $g(x)$. We tested with two slightly different readout procedures: one with a fixed readout time and another where the readout time was uniformly random within a final interval, forcing the network to maintain the correct output $g(x)$ across multiple steps. We considered two different target functions: $g(x) = \sin(x)$ for $x \in [0, 2\pi]$ and $g(x) = \tanh(x)$ for $x \in [-4, 4]$.

2.2.2 Maze navigation task

Maze navigation tasks have a long history in behavioral and systems neuroscience (Olton, 1979; Ainge et al., 2007). In our maze navigation task, the recurrent neural network acts as an instantaneous velocity controller for a particle in a fixed maze environment (Figure 3a). The objective is to navigate the particle from one maze vertex (the blue X's in Figure 3a), to another, pausing at the vertices along the way. The particle is perturbed by random velocity fluctuations that the network must reject as it navigates. In each trial, the starting and destination particle positions are sampled uniformly at random from the list of maze vertices. The networks receive constant inputs communicating the coordinates of their destination vertex, the current position of the particle, and an indication of whether the network should be paused at a vertex or traveling from one vertex to the next.

2.2.3 Single-neuron regulator task

To illustrate the effect of noise in a simpler task with fewer parameters so we could more easily isolate mechanisms, we consider a simple regulator task (Anderson & Moore, 2007), so simple that a network with only one neuron recurrently connected to itself, no inputs, and direct neural output (that is, the output is just the neural state h_t) can do it. In this single-neuron regulator task, the neural state must match a constant setpoint r in the presence of noise, which, with some added complexities, is also the essential objective of the function computation and maze navigation tasks. For our experiments with the single-neuron regulator task, we injected both pre- and post-activation noise, subsuming Equations 2 and 3 as special cases; we varied the proportion of these noise levels to observe how the loss function landscape varies as the noise goes from primarily pre-activation to primarily post-activation. As we will show, the noise type (e.g., pre- or post-activation) is a key independent variable in determining the final role of the noise in the trained networks. With only one neuron and no inputs or explicitly computed outputs, the only trainable parameters are the scalar recurrent weight and the scalar neural bias. The task itself is effectively parameterized by only two dimensionless parameters: the ratio of the pre-activation noise standard deviation to the post-activation noise standard deviation ($\sigma_{\text{in}}/\sigma_{\text{out}}$) and the ratio of the setpoint value to the post-activation noise standard deviation (r/σ_{out}).

3 Results

3.1 Function computation networks trained with noise inside, not outside, their activation functions require the noise for best performance.

We trained both noise-in and noise-out networks (Equations 2 and 3) on the function computation tasks and tested them under a range of noise levels, including zero noise at the low end. For noise-in networks, root

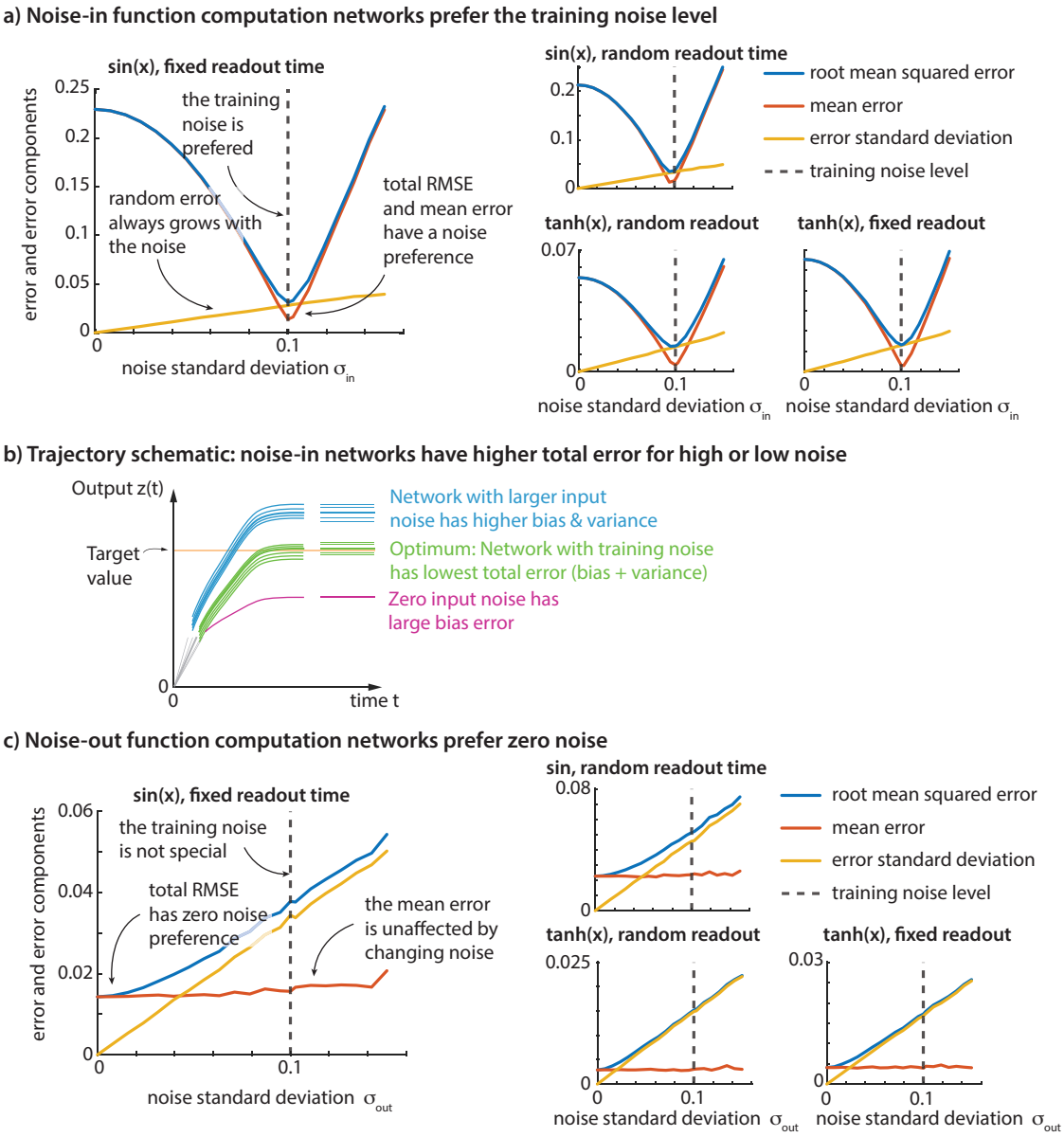

Figure 2: **Simple function computation: Noise-in networks prefer the training noise level, but noise-out networks prefer zero noise.** a) Root mean squared error, mean error, and error standard deviations for noise-in function computation networks. The best performance occurs when testing at or near the training noise level, and this preference is driven by a non-monotonic dependence between the noise level and the mean error (i.e., the systematic error). This indicates that passing the noise through the activation function somehow induces a noise-level-dependent systematic bias in the network outputs. b) Schematic illustrating that the network output trajectories with training noise has the lower total error compared to when noise is zero or higher. The mean trajectory is depicted by a thick line and individual realizations by thin lines. c) Root mean squared error, mean error, and error standard deviations for noise-out function computation networks. Unlike the noise-in networks, the noise-out networks perform best when tested with zero noise, and the systematic error appears unaffected by changes in the noise.

mean squared error (RMSE) was minimized when the test noise matched the training noise (Figure 2a-b). This shows that the noise does more than act as a regularizer: it becomes integral to the computation. In

contrast, noise-out networks performed best with zero noise (Figure 2c), consistent with the noise serving a purely regularizing role. In noise-in networks (Figure 2a-b), the increase in performance deficits away from the training noise levels were largely driven by bias rather than variance. While error variance grew roughly linearly with the variance of the injected noise, systematic error (bias) changed non-monotonically, being high for both zero noise and for noise much higher than training noise. The non-monotonicity in the bias error is qualitatively similar to the non-monotonicity in the total error, except that the bias error is minimized at a slightly higher noise level than the total error. This suggests that noise-dependent output biases, linked to the activation function, cause the observed preference.

3.2 Noise preference also emerges in more neuroscientifically relevant multi-task networks.

The maze navigation task confirmed that this effect generalizes beyond simple function approximation. Noise-in networks trained on the maze task also achieved their best performance when tested at the training noise level (figure 3). As for the function computation networks, deviations from the training noise produced performance deficits: this non-monotonicity of total error is largely driven by error bias, not error variance, showing that the noise preference mechanism persists in more realistic, neuroscientifically rich settings.

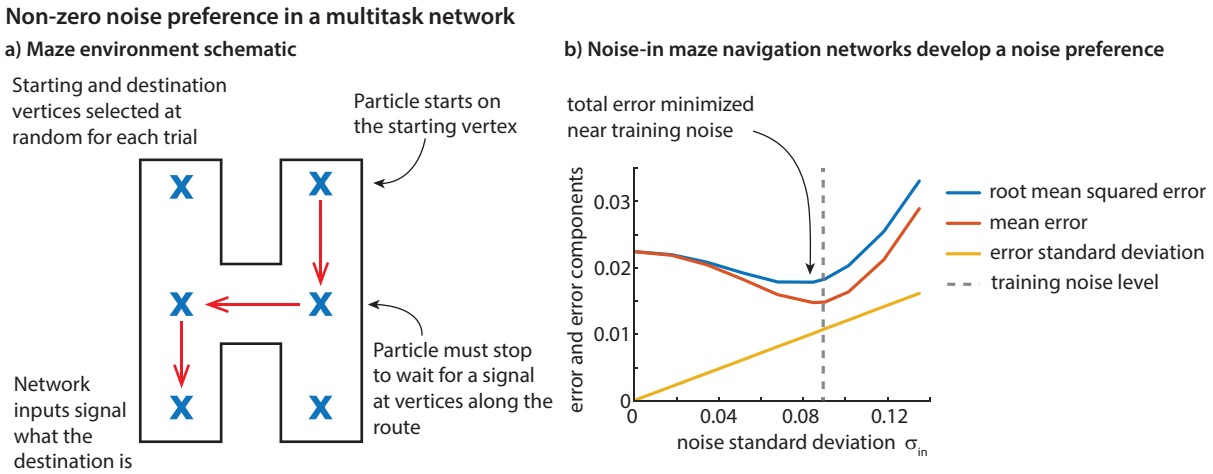

Figure 3: **Maze navigation task and results.** a) Schematic of the maze environment. The blue x's show the locations of maze vertices where the network has to stop and wait as it navigates from the start vertex to the destination vertex. The red arrows between vertices denote the multiple short jaunts that make up one of the routes through the maze. b) Root mean squared error, mean error, and error standard deviation for a noise-in maze navigation network when tested at a variety of different noise levels. As with the function computation networks, the network performs best at the training noise level, and the performance deficits at other noise levels are driven by error bias. For instance, setting noise to zero during test time results in the particle systematically falling short of its destination.

3.3 Fixed points of stochastic RNNs can be shifted by noise

Prior work has shown that CTRNNs solve tasks through low-dimensional dynamical features such as fixed points (Driscoll et al., 2024; Yang et al., 2019; Vyas et al., 2020). For a deterministic dynamical system with constant inputs, fixed points are invariant points in state space with $\dot{h} = 0$; that is, a network starting at a fixed point remains there forever in the absence of perturbations (e.g., point attractors are asymptotically stable fixed points). Both our function computation and maze tasks require maintaining static outputs over time, making asymptotically stable fixed points natural computational primitives. While there are no true fixed points for the stochastic neural networks (Equations 1-3), for these systems, we use "fixed point" to refer to the mean of the stationary distribution near point attractors.

In the following subsections, we first demonstrate how both pre- and post-activation noise can induce shifts in the effective fixed point locations of a noisy CTRNN. Then, in Section 3.4, we demonstrate that these shifts quantitatively predict noise-preference behavior, thus providing a dynamical mechanism for the phenomenon.

3.3.1 Noise can shift fixed points in noise-in networks

In noise-in networks, the activation function $f(\cdot)$ is applied after the noise samples are added to the summed and biased synaptic inputs, namely, $W_{\text{rec}}h_t + W_{\text{in}}u_t + B_{\text{in}}$ (Equation 2). Therefore, for a single neuron in a noise-in network that has settled into a stationary state distribution, the argument to the activation function will be a sum of samples from two distributions, one corresponding to the summed and biased synaptic input, which generally will come from a distribution with nonzero mean μ_s, and one corresponding to the injected noise, which by design will come from a distribution with zero mean $\mathcal{N}(0, \sigma_{\text{in}}^2)$). Ignoring the synaptic input variability, the excitatory term in the discrete update rule for this neuron is then proportional to: $f(\mu_s + \mathcal{N}(0, \sigma_{\text{in}}^2))$. (If we do not ignore variability in the synaptic input term, we can just lump that variability with the injected noise term to reach the same qualitative conclusions.) If μ_s is large in comparison to σ_{in} and negative, the noise will only very rarely push the argument of the activation function high enough to excite the neuron, effectively making it such that the noise does not affect this neuron. Similarly, if μ_s is large and positive, the noise will only very rarely push the argument of the activation function low enough to significantly involve the saturation of the activation function; this makes the noise act as excitation and inhibition in equal proportion, resulting in zero net effect on the expected state of the neuron. If $|\mu_s|$ is on the order of σ_{in}, however, the argument regularly fluctuates in and out of the saturated region, resulting in the selective attenuation of inhibitory noise samples. In this situation, the noise has a net excitatory effect on the expected activation level of the neuron, and this effect is σ_{in}-dependent (Figure 4a), because a larger σ_{in} results in more frequent, larger magnitude crossings into and out of the saturated region.

Expanding this reasoning to all the neurons in the network, we see that the locations of fixed points situated near boundaries between linear regions of the dynamics (where some neurons receive a net excitatory drive from the noise) are noise-level dependent. If the network has been fully optimized for some task that depends on the location of such a fixed point, we might expect noise level changes at test time to worsen performance.

3.3.2 Noise can shift fixed points in noise-out networks

Consider the piecewise-linear differential equation given by:

$$\dot{h} = \begin{cases} -\theta_{large}h + \sigma\eta & \text{when } \; x \geq 0 \text{ and} \\ -\theta_{small}h + \sigma\eta & \text{when } \; x > 0 \end{cases} \tag{4}$$

where $0 < \theta_{small} < \theta_{large}$, and η is a white noise process. This is a piecewise version of an Ornstein-Uhlenbeck (OU) process (Uhlenbeck & Ornstein, 1930), and we can implement it in a noise-out, one-neuron CTRNN with ReLU activation and no inputs or activation bias as follows:

$$\tau\frac{dh}{dt} = -h + \text{ReLU}(w_{\text{rec}}h) + \frac{\sigma}{\theta_{small}}\eta, \text{ with } \tau = \frac{1}{\theta_{small}}, \text{ and } w_{\text{rec}} = -\frac{\theta_{large} - \theta_{small}}{\theta_{small}} \tag{5}$$

In the absence of noise ($\sigma_{\text{out}} = 0$), this system has a single stable fixed point at $h = 0$ (i.e., its fixed point is exactly on the boundary between linear regions), but for $\sigma_{\text{out}} > 0$, the stationary distribution acquires an increasing positive shift as the noise level increases (Figure 4b). This is because noise-induced deviations in the positive direction persist for longer owing to the smaller decay rate on that side, and the larger the deviations are, the greater the discrepancy between the positive and negative decay times tends to be.

Similar to the situation for noise-in networks, this emergent shift in the stationary distribution depends on the fixed point being close to or coincident with the boundary between linear regions. If we add a large negative neural bias term inside the activation function in Equation 5, it would push the piecewise boundary to some large negative h value while leaving the fixed point at $h = 0$. In this situation, there would be a negligible noise-induced shift in the stationary distribution because the dynamics would become equivalent to the standard Ornstein-Uhlenbeck process except in the rare case of very large negative excursions from the fixed point. We would get a similar result if we included a large positive neural bias, but in that case,

both the piecewise boundary and the fixed point would move in the positive direction, but the boundary would move farther, producing a gap between the two.

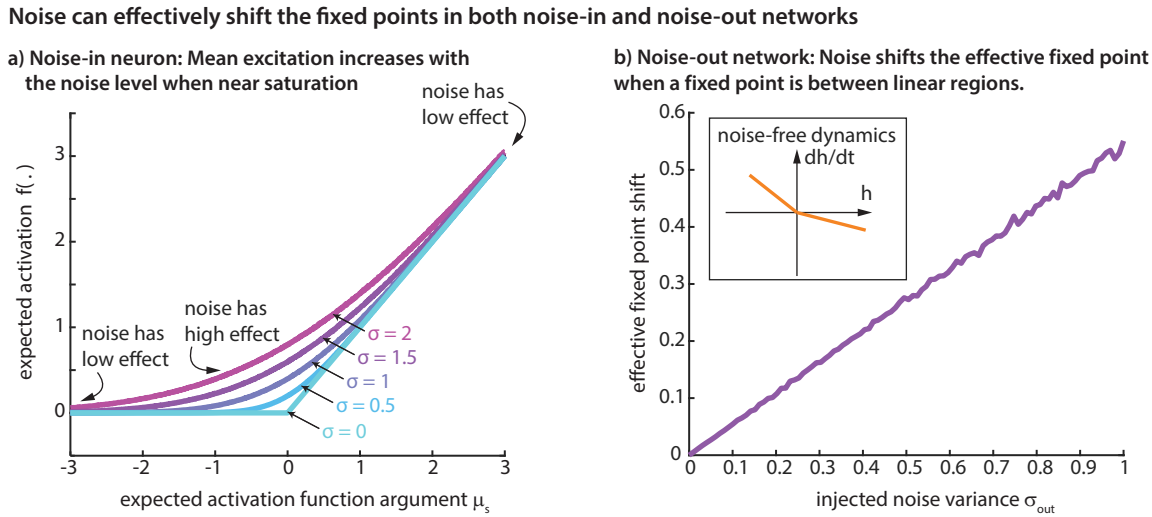

Figure 4: **Noise can shift the fixed points of both noise-in and noise-out networks if they have fixed points near a boundary between linear regions of their dynamics.** a) Functional relationship between the mean of a normal distribution before and after transformation by the ReLU activation function for multiple different standard deviations. When the absolute value of the mean is on the order of the standard deviation, interaction with the nonlinearity causes a variance-dependent positive shift in the mean of the transformed distribution. As a result, the locations of fixed points in a noise-in network will depend on the noise level if those fixed points are situated near boundaries between linear regions in the dynamics; a no-noise single-neuron version of such a noise-in network is shown as an inset. b) Functional relationship between the mean of the stationary distribution of a piecewise Ornstein-Uhlenbeck process (Equations 4 and 5) and the standard deviation of the noise. Inset shows a no-noise single-neuron version of such a noise-out network. As the standard deviation grows, the stationary distribution shifts in the positive direction because deviations in that direction take longer to decay. This single-neuron example illustrates why the locations of fixed points in a noise-out network depend on the noise level if those fixed points are situated near boundaries between linear regions.

3.4 Noise-induced fixed point shifts predict low-noise performance deficits

To investigate the possibility that fixed point shifts are responsible for the noise preference, we first computed the fixed points of our noise-in function computation networks, both with and without accounting for noise bias effects; see Appendix C for the fixed point finding procedure. We computed the difference between the zero noise and training noise fixed point locations, and we projected these training-noise-induced fixed point shifts by the transformation that produces the output ($z = W_{\text{out}}h + B_{\text{out}}$) to compute the resulting shifts in the output. We found that these output shifts approximately predict the input-specific error biases observed when testing the networks with zero noise (Figure 5).

3.5 Single-neuron regulator: noise inside the activation function alters the loss landscape to favor solutions that rely on noise-induced fixed point shifts

Since both noise-in and noise-out networks can exhibit noise-dependent fixed point shifts, but we only see a noise preference in noise-in networks, we hypothesized that there may be some performance incentive specific to noise-in networks that drives the development of a preference. Given our reasoning in sections 3.3.1 and 3.3.2, we sought to understand how the loss function varies with the distance between fixed points and

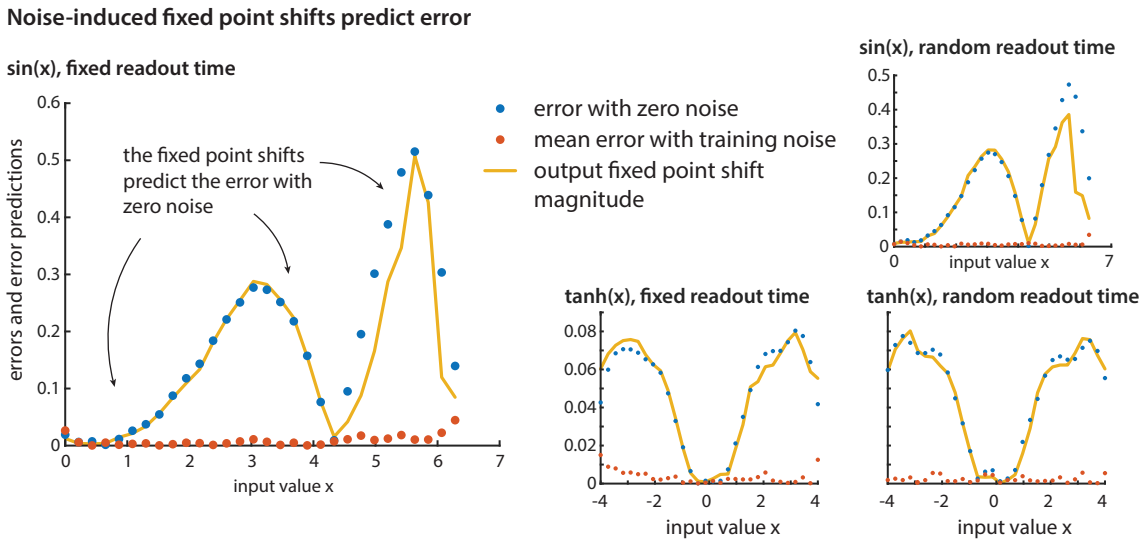

Figure 5: **Noise-induced fixed point shifts predict input-specific error in noise-in function computation networks tested with zero noise.** Noise induced fixed point shifts projected onto the output matrix closely track the zero noise error profile across the input domain, confirming that noise-induced fixed point shifts are responsible for the noise preference.

nonlinear boundaries in the dynamics. For simplicity, we use the single-neuron regulator task to investigate this.

In the single-neuron regulator task, the setpoint r determines where the neuron will attempt to center its stationary distribution. So by varying the setpoint, we control how close or far the stationary distribution is from the saturation of the activation function. Large positive setpoints encourage the stationary distribution to be far from the saturation (where we do not expect noise preference), while small positive setpoints encourage stationary distributions near the boundary of the saturation (where we may expect a noise preference). We trained many single-neuron regulators, each with a different combination of setpoint and pre-activation noise level, setting the post-activation noise level to one without loss of generality (implicitly scaling the problem by this noise level). This allows us to observe which setpoints permit the best performance given the relative strength of the pre- and post-activation noise streams. We optimize the bias for various fixed values of the recurrent weight, because training both the recurrent weight and the neural bias is ill-posed, resulting in unbounded recurrent weights.

The single neuron regulator experiments showed that there is a region in the parameter space where networks exhibit a noise preference. When the pre-activation noise dominates the post-activation noise, the best networks tend to land inside or near this region with a noise-preference, but when the post-activation noise dominates, they land squarely outside this region (Figure 6). We believe this trend is due to a tradeoff. If the stationary distribution straddles the saturation boundary, a portion of the pre-activation noise gets turned off, while leaving a portion of the post-activation noise out of reach for the recurrent weight to help in drawing the state back toward its expected value. For a network dominated by pre-activation noise, this is a good trade, so the stationary distribution should be placed near the boundary, but for a network dominated by post-activation noise, this is a bad trade, so the stationary distribution should be placed far from the boundary. Given the reasoning in sections 3.3.1 and 3.3.2, this may explain why noise-in networks systematically develop a noise preference while noise-out networks do not.

4 Discussion

Using a simple function computation framework and a maze navigation framework as illustrative examples, we have shown that noisy CTRNNs sometimes develop a preference for the specific noise level used during

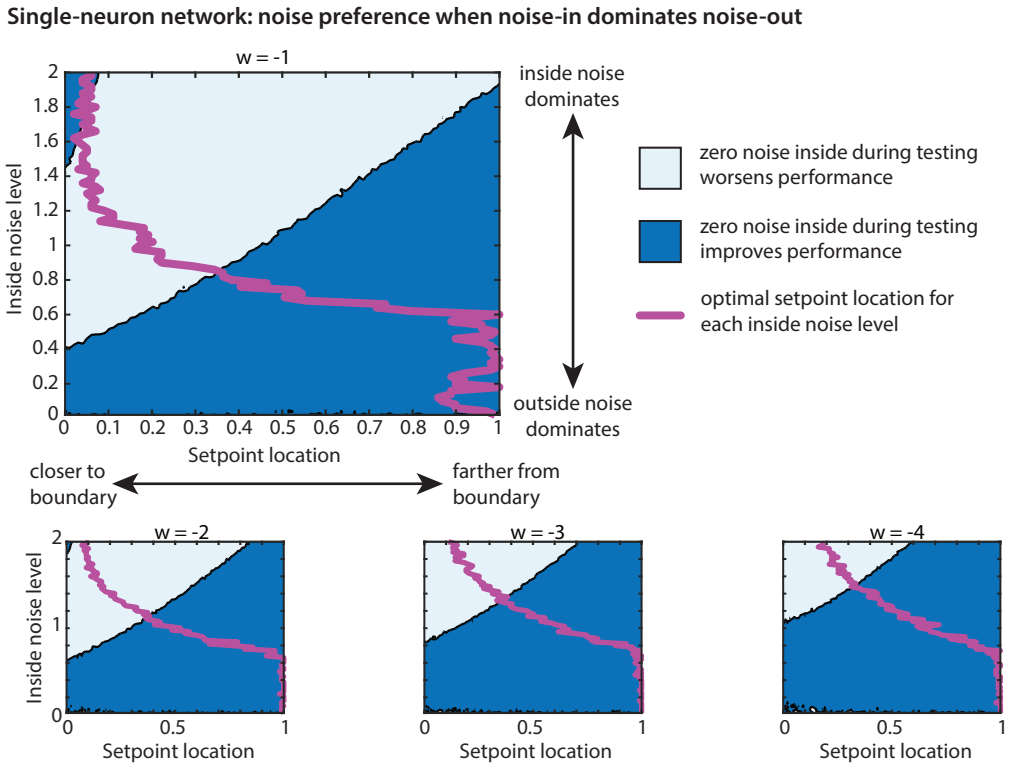

Figure 6: **Single neuron regulator experiments show that increasing inside noise-level encourages setpoints closer to the saturation boundary** As the pre-activation noise grows in relation to the post-activation noise, the optimal setpoint gets closer to the saturation boundary, eventually getting close enough to produce a noise preference. This is true for all values of the recurrent weight, w, that we sampled. This explains why we only see a noise preference in the noise-in function computation networks.

training, where any change in the noise level at test time results in worse performance. When noise is injected before the application of the activation function, the networks tend to develop a noise preference, but when noise is injected after, they do not. By analyzing the fixed points of the noise-in function computation networks, we found that the noise preference is driven by noise-variance-dependent shifts in the stationary neural state distributions. These shifts are caused by inhomogeneous noise attenuation that only occurs when the neural state is near a boundary between linear regions of the network dynamics. Though the locations of the stationary distributions of both noise-in and noise-out networks will depend on the noise if they are placed near such boundaries, experiments with a single-neuron regulator problem showed that only the noise-in networks have a performance incentive to do so, thus explaining why only the noise-in networks developed a noise preference.

4.1 Relation to phenomena like stochastic resonance

We have presented a phenomenon involving an optimal, nonzero noise level, but the phenomenon we outline here is distinct from the well-known stochastic resonance (McDonnell & Abbott, 2009), and other similar phenomena such as coherence resonance (Pikovsky & Kurths, 1997; Hutt et al., 2020), and recurrence resonance (Katada & Nishimura, 2009; Metzner et al., 2024; Krauss et al., 2019). Speaking broadly, these phenomena apply to scenarios where a system's behavior can be described in terms of transitions between macro-states that are separated by thresholds (e.g., distinct attractors, regimes on either side of a bifurcation, half-spaces on either side of a detection threshold, etc.), and the performance criterion depends (either implicitly or explicitly) on both a measure of the ease with which the system makes transitions between macro-states and some measure of predictability. The role of the noise in these systems is to provide a

constant stream of disturbances that can nudge the system across transition thresholds, and the existence of an optimal nonzero noise level stems from the tension between ease of transitions and predictability of the system: in the simplest version of stochastic resonance, detection of a weak sub-threshold signal is enabled by the addition of noise. Although our phenomenon arises from a vaguely similar tension (the networks learn to optimally trade neural coupling for a reduction in neural variance by operating neurons near saturation), the optimality of the noise for our networks is a byproduct of the optimality of our networks for the noise: that is, it is an over-fitting phenomenon. In contrast, the resonance phenomena only occur in systems that are overall suboptimal for the objective, in that one could improve performance in a system exhibiting a resonance phenomenon by altering system parameters other than the noise level (to our knowledge this has only been explicitly discussed in the literature for stochastic resonance (Tougaard, 2000), but likely also the case for the other resonance phenomena mentioned above).

4.2 Future work

We have shown that a noise preference emerges in noise-in networks trained on a few different tasks, but all of our tasks hinge on stabilizing network outputs around constant setpoints. As a result, our networks ended up relying on fixed points or point attractors (Khona & Fiete, 2022) to implement their computations, and our explanation for the noise preference phenomenon is predicated on this reliance. However, many tasks require more than just stabilizing outputs around setpoints. One example is locomotion, where the outputs should exhibit the characteristics of a stable periodic motion or limit cycle (Seethapathi & Srinivasan, 2019; Laszlo et al., 1996), not a point attractor. Future work should examine a wider range of such tasks not easily solved by point attractor dynamics.

Our numerical experiments used additive Gaussian noise. Although additive Gaussian noise is common in the literature (e.g., Yang et al. (2019); Driscoll et al. (2024)), explicitly signal-dependent noise models, such as multiplicative noise or Poisson noise, may be an important aspect of the noise environment of biological systems (Jones et al., 2002; Tolhurst et al., 1983; Medina, 2011). Our explanation for the noise preference phenomenon depends on an induced signal dependence in the noise distribution: for neurons near saturation, the portion of the noise attenuated by the activation function depends on the net synaptic drive. So, other signal-dependent noise models could also result in a preference for specific noise parameters. Indeed, in the standard implementation of dropout (Srivastava et al., 2014), perhaps one of the most widely used signal-dependent noising procedures in the literature, a necessary step is to weight the layer outputs by the dropout probabilities, so that the dropout fraction can be set to zero at test time without degrading performance. Future work should investigate the potential for noise preference phenomena when using a variety of signal-dependent noise models.

References

J A Ainge, M A Van Der Meer, R F Langston, and E R Wood. Exploring the role of context-dependent hippocampal activity in spatial alternation behavior. *Hippocampus*, 17(10):988–1002, 2007.

B D O Anderson and J B Moore. *Optimal Control: Linear Quadratic Methods*. Dover Books on Engineering. Dover Publications, 2007. ISBN 9780486457666. URL `https://books.google.com/books?id=fW6TAwAAQBAJ`.

O Barak. Recurrent neural networks as versatile tools of neuroscience research. *Current opinion in neurobiology*, 46:1–6, 2017.

Chris M Bishop. Training with noise is equivalent to tikhonov regularization. *Neural computation*, 7(1): 108–116, 1995.

L N Driscoll, K Shenoy, and D Sussillo. Flexible multitask computation in recurrent networks utilizes shared dynamical motifs. *Nature Neuroscience*, 27(7):1349–1363, 2024.

A A Faisal, L P J Selen, and D M Wolpert. Noise in the nervous system. *Nature reviews neuroscience*, 9(4): 292–303, 2008.

V Goudar, B Peysakhovich, D J Freedman, E A Buffalo, and X-J Wang. Schema formation in a neural population subspace underlies learning-to-learn in flexible sensorimotor problem-solving. *Nature Neuroscience*, 26(5):879–890, 2023.

U Güçlü and M A J Van Gerven. Modeling the dynamics of human brain activity with recurrent neural networks. *Frontiers in computational neuroscience*, 11:7, 2017.

A Hutt, J Lefebvre, D Hight, and H A Kaiser. Phase coherence induced by additive gaussian and non-gaussian noise in excitable networks with application to burst suppression-like brain signals. *Frontiers in Applied Mathematics and Statistics*, Volume 5 - 2019, 2020. ISSN 2297-4687. doi: 10.3389/fams.2019.00069. URL `https://www.frontiersin.org/journals/applied-mathematics-and-statistics/articles/10.3389/fams.2019.00069`.

K E Jones, A F C Hamilton, and D M Wolpert. Sources of signal-dependent noise during isometric force production. *Journal of neurophysiology*, 88(3):1533–1544, 2002.

N Katada and H Nishimura. Stochastic resonance in recurrent neural network with hopfield-type memory. *Neural processing letters*, 30:145–154, 2009.

M Khona and I R Fiete. Attractor and integrator networks in the brain. *Nature Reviews Neuroscience*, 23 (12):744–766, 2022.

D P Kingma. Adam: A method for stochastic optimization. *arXiv preprint arXiv:1412.6980*, 2014.

P Krauss, K Prebeck, A Schilling, and C Metzner. Recurrence resonance" in three-neuron motifs. *Frontiers in computational neuroscience*, 13:64, 2019.

J Laszlo, M van de Panne, and E Fiume. Limit cycle control and its application to the animation of balancing and walking. In *Proceedings of the 23rd annual conference on Computer graphics and interactive techniques*, pp. 155–162, 1996.

S H Lim, N B Erichson, L Hodgkinson, and M W Mahoney. Noisy recurrent neural networks. *Advances in Neural Information Processing Systems*, 34:5124–5137, 2021.

M D McDonnell and D Abbott. What is stochastic resonance? definitions, misconceptions, debates, and its relevance to biology. *PLoS computational biology*, 5(5):e1000348, 2009.

J M Medina. Effects of multiplicative power law neural noise in visual information processing. *Neural computation*, 23(4):1015–1046, 2011.

C Metzner, A Schilling, A Maier, and P Krauss. Recurrence resonance-noise-enhanced dynamics in recurrent neural networks. *Frontiers in Complex Systems*, 2:1479417, 2024.

H Noh, T You, J Mun, and B Han. Regularizing deep neural networks by noise: Its interpretation and optimization. *Advances in neural information processing systems*, 30, 2017.

D S Olton. Mazes, maps, and memory. *American psychologist*, 34(7):583, 1979.

A S Pikovsky and J Kurths. Coherence resonance in a noise-driven excitable system. *Phys. Rev. Lett.*, 78:775–778, Feb 1997. doi: 10.1103/PhysRevLett.78.775. URL `https://link.aps.org/doi/10.1103/PhysRevLett.78.775`.

N Seethapathi and M Srinivasan. Step-to-step variations in human running reveal how humans run without falling. *elife*, 8:e38371, 2019.

N Srivastava, G Hinton, A Krizhevsky, I Sutskever, and R Salakhutdinov. Dropout: a simple way to prevent neural networks from overfitting. *The journal of machine learning research*, 15(1):1929–1958, 2014.

D J Tolhurst, J A Movshon, and A F Dean. The statistical reliability of signals in single neurons in cat and monkey visual cortex. *Vision research*, 23(8):775–785, 1983.

J Tougaard. Stochastic resonance and signal detection in an energy detector–implications for biological receptor systems. *Biological Cybernetics*, 83(5):471–480, 2000.

G E Uhlenbeck and L S Ornstein. On the theory of the brownian motion. *Phys. Rev.*, 36:823–841, Sep 1930. doi: 10.1103/PhysRev.36.823. URL `https://link.aps.org/doi/10.1103/PhysRev.36.823`.

S Vyas, M D Golub, D Sussillo, and K V Shenoy. Computation through neural population dynamics. *Annual review of neuroscience*, 43(1):249–275, 2020.

P Y Wang, Y Sun, R Axel, L F Abbott, and G R Yang. Evolving the olfactory system with machine learning. *Neuron*, 109(23):3879–3892, 2021.

G R Yang and M Molano-Mazón. Towards the next generation of recurrent network models for cognitive neuroscience. *Current opinion in neurobiology*, 70:182–192, 2021.

G R Yang, M R Joglekar, H F Song, W T Newsome, and X-J Wang. Task representations in neural networks trained to perform many cognitive tasks. *Nature neuroscience*, 22(2):297–306, 2019.

Z You, J Ye, K Li, Z Xu, and P Wang. Adversarial noise layer: Regularize neural network by adding noise. In *2019 IEEE International Conference on Image Processing (ICIP)*, pp. 909–913. IEEE, 2019.

A Training details

All training was done in MATLAB using the ADAM optimization algorithm (Kingma, 2014) with learning rate decay. For the function computation and single-neuron regulator networks, we used an initial learning rate of 0.001, a momentum weight of 0.9, an RMSprop weight of 0.999, and $\epsilon = 10^{-7}$. The learning rate half-lives were 2,500 batches for the function computation networks and 4,545 batches for the single-neuron networks; both were trained for a total of 10,000 batches. For the function computation networks, we used a batch size of 32 trials, and for the single-neuron networks, we used a batch size of one. There was no explicit regularization in these networks except for noise injection, either inside or outside the activation function for the function computation networks, and both inside and outside in different proportions for the single-neuron networks. For the function computation networks, we used a fixed noise standard deviation of 0.1, regardless of whether the noise was injected inside or outside the activation function. To initialize networks other than single-neuron regulator networks, we set all biases to zero and we set all weights to be normally distributed with zero mean and standard deviation equal to $0.8/\sqrt{\#\ of\ neurons}$ (Driscoll et al., 2024; Yang et al., 2019). For the function computation networks, we used 100 neurons. For the single-neuron regulator networks, the only trained parameter was the bias, and we initialized it to be equal to $r(1-w)$, which places the fixed point of the deterministic dynamics (of which there was only one, because all sampled weights were negative) exactly equal to the setpoint r. The initial neural activation states of the function computation networks were trained parameters set to zero at the start of training. For the regulator networks, the initial neural state was equal to the setpoint.

For the maze navigation network, we used an initial learning rate of 0.004 and a learning rate half-life of 1,500 batches, with the other ADAM parameters the same as for the function computation and single-neuron regulator networks. The maze network was larger than the function computation networks, with 672 neurons, but we trained for fewer batches, only 6,000 (this specific network size is not necessary for the noise preference phenomenon; it was inherited from unrelated work involving spatial embedding of neurons, for which this size was convenient). The batch size was 36, with any combination of starting and ending vertices equally likely and heterogeneous within a batch. Unlike for the other networks, we used some explicit regularization on the square of the maximum singular value of the recurrent weight matrix to protect against dynamical and numerical instability during training (e.g., Goudar et al. (2023)). We implemented this by adding the following term to the loss function:

$$\left(\max \frac{\|W_{\text{rec}} v\|}{\|v\|}\right)^2 \tag{6}$$

We added this term to the loss function with a scaling coefficient of 0.001. In addition to this explicit regularization, we also injected Gaussian noise inside the activation function with zero mean and standard

deviation equal to 0.0894. The maze network had multiple trainable initial neural states (one for each vertex in the maze, with the initial state selected based on which vertex the trial starts on), each of which was set to the zero vector at the start of training.

All networks used ReLU or the SoftPlus activation function. The SoftPlus activation function is defined as:

$$\text{SoftPlus}(\cdot) = \ln(1 + e^{\alpha(\cdot)})/\alpha, \tag{7}$$

where α is a scaling factor that controls the sharpness of the transition between the flat and sloped half-spaces. As α goes to infinity, the SoftPlus function approaches the ReLU function. For all networks in this paper, unless otherwise specified, we used $\alpha = 10$.

B Task details

B.1 Function computation

In the function computation tasks, we trained the networks to compute either the sine function over the interval $[0, 2\pi]$ or the hyperbolic tangent function over the interval $[-4, 4]$. In either case, the networks receive a one-dimensional input corresponding to the argument of the function being approximated, and their input remains on throughout the entire trial, so there was no requirement for the networks to "remember" the input. All trials lasted a total of 100 timesteps. In the deterministic readout variant of this task paradigm, the network output was read in the final time step for comparison to the target value; in the random readout variant, the readout could be read at any time step in the interval [70, 100] with equal probability, forcing the network to maintain the correct output over that entire interval. In implementing the random readout version of the task, we found that the networks learned more quickly if we considered two readout times, one in the final time step and one randomly distributed over a fraction of the total duration, as previously described. The loss function for these tasks was the root mean squared error between the target values and the network outputs at readout times.

B.2 Maze navigation

In the maze navigation task, we trained the network to navigate between any pair of vertices in a maze like the one shown in Figure 3a, pausing on vertices along the way. The network needed to pause on each vertex for a uniformly random number of timesteps, forcing it to rely on its inputs to determine when it should fixate at a maze vertex or move to the next. We loosely modeled the maze navigation framework after the multitask frameworks of Driscoll et al. (2024) and Yang et al. (2019) in the computational neuroscience literature. The network received three kinds of input: particle position state feedback, the destination indicator, and the fixation indicator. The particle state feedback was a 2-dimensional vector reporting the Cartesian coordinates of the particle in space in the current timestep. The destination indicator was a 2-dimensional vector indicating the Cartesian coordinates of the final destination vertex in space, and the fixation indicator was a 2-dimensional one-hot vector with both elements set to zero unless the network should be paused at a vertex. In timesteps when the network should be paused on the starting vertex of a trial, the first element of the fixation vector was set to one, and in timesteps when the network should be paused at any other vertex along the route, the second element was set to one. The network output was the instantaneous velocity of the particle, represented in 2-dimensional Cartesian coordinates. To force the network to learn to stabilize the particle along the maze routes, zero-mean Gaussian noise with variance equal to 0.0005 in each dimension was added to the network output in each time step, making it such that the particle would do a random walk if the network output were zero.

At the start of a trial, the particle position is initialized at one of the vertices, and the network state is initialized accordingly (see section A). In the first 20 timesteps, a period we refer to as the downtime period, the second element of the fixation vector is on, and the destination indicator shows the coordinates of the starting maze vertex, making the input conditions identical to if we had just finished a route terminating at the current starting vertex. Then, over a period with length uniformly distributed in $[30, 50]$ timesteps, which we call the starting fixation period, only the first element of the fixation vector is on, and the destination vector shows the coordinates of the destination for the present trial, which is how it will remain for the

remainder of the trial. During the downtime and starting fixation periods, the network must remain a the starting maze vertex. The rest of the trial then alternates between jaunt periods, intervals 20 timesteps long when both elements of the fixation vector are set to zero and the network must navigate the particle to the next vertex along the route, and via fixation periods, which have length distribution identical to that of the starting fixation period, and during which only the second element of the fixation vector is turned on. For computational efficiency, we buffered out all trials to be 280 steps long, regardless of how long their corresponding routes were. To do this, we added extra time steps to one of the fixation periods at random, so there was a chance that any one pause could exceed the intervals previously given. loss function for the maze task was the root mean squared error between the particle position and its target position over all timesteps and trials in a batch. The target position for the particle during pauses was simply the vertex position at which it was supposed to be pausing, and during jaunt periods, we used a smooth cubic polynomial interpolator between the starting and ending vertices of the jaunt, constraining the starting and ending velocities of the jaunt to be zero.

B.3 Single-neuron regulator

The scalar neural state h_t of the single-neuron CTRNN with noise both inside and outside its activation function has dynamics defined by the update rule:

$$h_{t+1} = (1-\gamma)h_t + \gamma(\mathrm{ReLU}(wh_t + b + \mathcal{N}(0, \sigma_{\mathrm{in}}^2)) + \mathcal{N}(0, \sigma_{\mathrm{out}}^2)) \text{ with } h_1 = r. \tag{8}$$

We considered the regulator problem (Anderson & Moore, 2007) described by the loss function:

$$\min \frac{1}{T}\sum_{t=1}^{T}(h_t - r)^2, \tag{9}$$

where $r \geq 0$ is the constant setpoint for h_t. We fixed σ_{out} (the noise standard deviation outside the activation function, set to one), T (the number of simulation time steps, set to 50) and γ (the ratio of the simulation timestep to the neural time constant, set to 0.2), and found the optimal value of b (the activation bias) for different combinations of w (the recurrent weight), σ_{in} (the noise level inside the activation function), and r (the setpoint). We then measured the difference in performance between when σ_{in} is left at the value for which the networks were optimized and when it is set to zero. For each combination of w and σ_{in}, we also identify the value of the setpoint r that permits the lowest loss function value among those we sampled. We considered a fine sampling of 100 values for both r (evenly spaced in the interval [0,1]) and σ_{in} (evenly spaced in the interval [0,2]), and we considered four values of w, namely $\{-1, -2, -3, -4\}$, with the largest magnitude $w = -4$ selected such that the deterministic dynamics would extinguish any deviation from the fixed point in a single time step if there were no noise. We set the post-activation noise level to one for all experiments while varying the setpoint location and the inside noise level, without loss of generality, because the fixed point shift phenomenon depends on how far a fixed point is from nonlinear boundaries *in comparison to* the noise standard deviation.

C Fixed point finding with and without noise

To find the fixed points of the noise-in function computation networks without accounting for noise-induced shifts (Driscoll et al., 2024), we optimized the following objective function with respect to the neural state h:

$$\|\gamma(-h + f(W_{\mathrm{rec}}h + W_{\mathrm{in}}u + B_{\mathrm{in}}))\|^2. \tag{10}$$

This objective function is simply the squared magnitude of the discrete change in h if we take a single simulation step starting from h, so its local minima correspond to locations in the neural activation space where the network state changes most slowly in a local neighborhood. We optimized this objective using ADAM with learning rate decay, using an initial learning rate of 0.07, a momentum weight of 0.9, an RMSprop weight of 0.999, $\epsilon = 10^{-7}$, and a learning rate half-life of 1,386 optimization steps. We terminated the optimization when the objective dropped below 4.9×10^{-9}. To find the fixed point corresponding to a particular argument of the function to be approximated by the network, we ran the network without noise

over a full trial with that argument, taking the final neural state as the initial guess for the fixed point, and then we optimized the objective function with u set to the argument of interest.

To find the fixed points of the noise-in function computation networks with noise accounted for, we followed the same procedure as for the noise-free fixed points, but using the following cost:

$$\|\gamma(-h + E(f(W_{\text{rec}}h + W_{\text{in}}u + B_{\text{in}} + \mathcal{N}(0, \sigma^2)))\|^2, \tag{11}$$

where $E(\cdot)$ denotes a Monte Carlo approximation of the expected value, evaluated by averaging over 300 samples, and σ is the noise standard deviation used during network training, equal to 0.1. For these optimizations, we used the same optimization parameters as for the noiseless procedure, except we used an initial learning rate of 0.0175, and we terminated the optimization when the objective function dropped below $\frac{1}{100}\sigma^2(\#\ \text{of neurons})/(\#\ \text{of noisy samples}) = \frac{1}{3} \times 10^{-4}$.

To compute the magnitude of the output fixed point shift induced by the noise, we simply took the difference between the noisy fixed point and the noise-free fixed point corresponding to each input argument, left-multiplied it by the output matrix W_{out}, and took its magnitude.